



Thermal Management Techniques for Concentrating Photovoltaic Modules

9

Xiaoru Zhuang, Xinhai Xu, and Jianpeng Cui

Contents

9.1	Introduction	248
9.2	Passive Cooling	249
9.2.1	Natural Convection Heat Sink Cooling	249
9.2.2	Heat Pipe Cooling	251
9.2.3	Phase Change Material (PCM) Cooling	254
9.3	Active Cooling	256
9.3.1	Jet Impingement Cooling	256
9.3.2	Liquid Immersion Cooling	257
9.3.3	Microchannel Heat Sink Cooling	262
9.4	Discussion and Conclusion Remarks	264
	References	276

Abstract

Concentrating photovoltaic technology is one of the most promising solar energy utilization technologies which can directly transform sunlight into electricity with high conversion efficiency up to 46%. Nevertheless, the concentrator brings a large amount of heat to the solar cell and temperature of the solar cell significantly affects its performance by reducing the efficiency and lifespan. Therefore, it is

X. Zhuang · J. Cui

School of Mechanical Engineering and Automation, Harbin Institute of Technology, Shenzhen, China

X. Xu (✉)

School of Mechanical Engineering and Automation, Harbin Institute of Technology, Shenzhen, China

Institute of Hydrogen and Fuel Cell, Harbin Institute of Technology, Shenzhen, China
e-mail: xuxinhai@hit.edu.cn

necessary to use proper cooling technology to dissipate the excess heat and maintain the solar cell temperature in an acceptable range. This work presents an overview of various cooling technologies available for concentrating photovoltaic systems in terms of passive and active methods. In passive cooling, natural convection heat sink cooling, heat pipe cooling, and phase change material cooling have been summarized. Inactive cooling, jet impingement cooling, liquid immersion cooling, and microchannel heat sink cooling have been evaluated. At last, discussions of these cooling techniques were reviewed.

9.1 Introduction

The photovoltaic (PV) cell is one of the most widespread renewable energy power generation technologies which can directly transform sunlight into electricity. The main challenge of PV cell commercialization is the high initial cost compared to conventional fossil sources-based power generation technologies [1, 2]. In order to increase the efficiency of PV power generation and make it more cost effective, concentrating photovoltaic (CPV) was proposed by using cheaper concentrating mirrors or lenses to capture the incident solar irradiance on a relatively large area and concentrate that energy onto small solar cell (SC) [3, 4]. The new world efficiency record of a CPV is up to 46% reported by Soitec and French Commission for Atomic Energy and Alternative Energies (CEA) – Laboratoire d'électronique des technologies de l'information (Leti), together with the Fraunhofer Institute for Solar Energy Systems (Fraunhofer ISE) and confirmed by Association for Iron & Steel Technology (AIST) in Japan [5], whereas non-concentrated photovoltaics (PVs), in general, have an efficiency of less than 25% [6]. According to the concentration ratio (CR) of a solar radiation incident, concentrating photovoltaic (CPV) systems can be classified under CR varying from 1 to 40 Suns [2.3 kW] for low, 40 to 300 Suns for medium, and 300 to 2000 Suns [100 kW] for high concentrating systems [7]. The ratio in “Suns” indicates the number of times the solar radiation is concentrated.

In a CPV system, only a fraction of incoming sunlight is converted into electricity, and the remaining solar energy is converted into heat [8]. The temperature of the PV cells can increase significantly without cooling. The cell efficiency is adversely influenced by the increasing temperature. Moreover, the high temperature can cause long-term degradation and irreversible structural damages to the cell such as deformation on the cell surface, delamination of the transparent layer, and development of micro-cracks on the cell [1, 9]. The temperature coefficient of conversion efficiency for most silicon SCs with a base temperature of 25 °C has been summarized by Skoplaki and Palyvos [10]. They reported that the average decrease in efficiency is around 0.45%/°C rise in operating temperature. Multi-junction (MJ) SCs are recently favored over single junction cells to be integrated into CPV systems as they are more efficient, have a better response to high concentration, and lower temperature coefficient [11]. Nashik et al. [12] reported the temperature coefficient of conversion

efficiency for [indium gallium phosphide/indium gallium arsenide/gallium] InGaP/In GaAs/Ge triple-junction SCs to be decreased by 0.248% at 1 Sun and 0.098% at 200 Suns for per degree rise in operating temperature. It is evident that thermal management of CPV systems plays a key role to improve the efficiency and life span of the SCs. Thus, it is necessary to introduce effective cooling technologies to dissipate heat, attain the higher performance, and prolong the lifetime of cells.

The following two sections will present and summarize current works in CPV cooling technologies in terms of passive cooling and active cooling. Passive cooling requires neither maintenance nor use of energy consuming devices such as pumps or fans, which are more reliable and cost-effective. In this section, natural convection heat sink cooling, heat pipe cooling, and phase change material (PCM) cooling methods will be summarized. Active cooling requires external energy to cool the SCs but is independent of the ambient conditions, so is usually easily controllable than passive cooling. In this section, it mainly evaluates the methods of jet impingement cooling, liquid immersion cooling, and microchannel heat sink cooling. Based on these efforts, discussions of those cooling techniques were reviewed for CPV cooling technologies.

9.2 Passive Cooling

9.2.1 Natural Convection Heat Sink Cooling

Heat sink with or without fins is one of the most common passive cooling solution applied in CPV systems [8]. It utilizes the effects of natural convection and radiation to dump waste heat for CPV by attaching the heat sink to the bottom of the cell (or cells). Araki et al. [13] conducted the outdoor experiments of a heat sink cooling for CPV systems at the concentration ratio of 500 Suns. They used an aluminum plate as the heat sink with a heat conductive epoxy and copper sheet between the SCs and metal plate. The results presented that the cell temperature only rose 18 °C under 500 Suns and 21 °C under 400 Suns to the ambient. Chou et al. [14] also numerically investigated the thermal performance of a high CPV system using an aluminum plate as the heat sink for cooling. The effects of the thickness of the heat sink, the thermal conductivity of the test board and solder paste of SCs assembly were discussed. The results showed that the thermal conductivity of the test board and solder paste had a slight effect to reduce cell temperature. However, the thickness of the heat sink played an important role in the thermal management of high CPV systems. The maximum cell temperature decreased as the aluminum thickness increased and became stable when the thickness was more than 20 mm. In order to predict the practical limits of flat plate cooling systems in natural convection for high CPV modules, Guladi et al. [15] proposed a thermal analytical model with the flat plate made of aluminum and a thickness of 3 mm. They found that flat plate systems cooled by natural convection of ambient air were sufficient to maintain the cell temperature below 80 °C up to CR of a few thousand Suns in the case of SCs side lengths of 2–4 mm and flat plate side lengths of 0–60 mm. Cui et al. [16] also

proposed a thermal model based on the energy conservation principle for CPV cells cooled by aluminum plates with a black coating as heat sinks. The heat sink area was 700 times larger than the area of SCs. According to the model, the cell temperature reduced as the heat sink area increased for a fixed CR. And for a certain fixed cell temperature, the heat sink area needed to increase linearly as a function of the concentration ratio. This model was verified by an outdoor experiment which measured the SCs temperature of 37 °C at the concentration ratio of 400 Suns.

Heat sink with fins can obviously increase the heat transfer surface area which remarkably enhances the thermal performance. Natarajan et al. [17] numerically studied the thermal performance of a CPV system cooling by a heat sink with and without fins. A two-dimensional (2-D) thermal model was developed to predict the SCs temperature. Based on the model, the SCs temperature with fins was significantly decreased compared to without fins. And they found that four uniform fins of 1 mm thickness and 5 mm height could effectively reduce the SCs temperature to 49.6 °C for CPV system at the concentration ratio of 10 Suns and ambient temperature of 20 °C. Aldossary et al. [11] also numerically investigated the feasibility of heat sink for passive cooling to maintain a single MJ PV cell surface temperature and electrical performance under high solar concentration in the harsh environment where ambient temperature could reach 50 °C. Two heat sink designs (shown in Fig. 9.1), namely, round pin heat sink (RPHS) and straight fins heat sink (SFHS), were simulated with the concentration ratio of 500 Suns. The results showed that SFHS had a better performance with the PV surface temperature of 21 °C lower than RPHS in ambient temperatures of 25–50 °C. The round pin heat sink was unable to keep the PV surface temperature below 80 °C at all test ambient temperatures and SFHS only could maintain the maximum PV surface temperature within the operating limit at an ambient temperature lower than 35 °C.

Micheli et al. [18] first used the least-material approach to design a heat sink for ultrahigh CPVs (concentration ratio over 2000 Suns). This method showed the potential to handle the thermal management of ultrahigh CPV systems, meanwhile limiting the costs and weight of the heat sink. The results showed that an 8-in × 11 cm wide × 6 cm high heat sink made of aluminum was able to keep a 3 mm × 3 mm MJ cell temperature below 80 °C at the concentration ratio of 4000

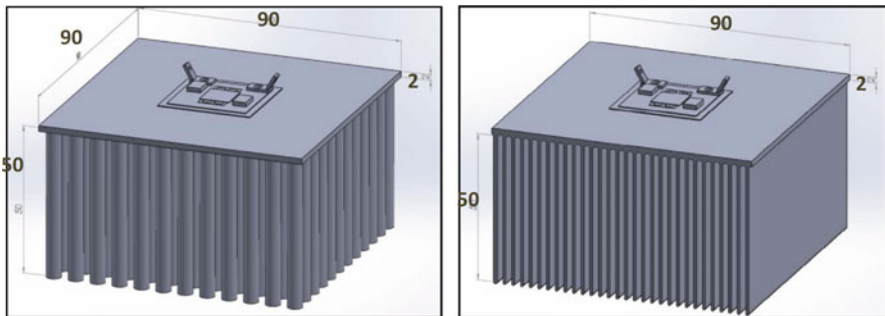


Fig. 9.1 Two heat sink structures investigated in Ref. [11], (a) RPHS, (b) SFHS

Suns. And it was concluded that the normalized cost of 0.1–0.18 \$/W_p was expected for production of optimized heat sinks for ultrahigh CPV systems at the concentration ratio from 1000 to 8000 Suns. Later, they optimized the least-material approach by reducing the heat sink baseplate extension and developed a 7-in × 9.6 cm wide × 5.62 cm high heat sink maintaining the cell temperature below 80 °C with a drop in weight and price of 61% [19]. Moreover, Micheli et al. [20] also investigated the feasibility of silicon micro-finned heat sinks for passive cooling of 500 Suns CPV systems by a simulation model. It was found that the SC temperature was lower than 80 °C by using a silicon wafer as a heat sink for both unfinned and finned conditions. And the fins performed better. The results showed that the application of micro-fins for passive cooling of CPV had the potential to reduce the material usage, the installation costs, and the tracker's energy consumptions, contributing to increasing the cost competitiveness of CPV in the renewable energy market.

For the purpose of estimating the thermal performance of a natural convective heat sink with fins for high CPV module cooling, Do et al. [21] proposed a general correlation based on extensive experimental data. And comparing with the previous studies [22, 23], the proposed correlation well predicted the effects of inclination angle and fin spacing on the thermal performance of the heat sink with plate-fins. They found that the optimal fin spacing strongly depended on the inclination angle and temperature difference for a specific geometry. The major problem related to the present natural convective heat sink cooling systems for heliostat concentrator photovoltaic (HCPV) is their heat dissipation efficiencies highly rely on the ambient temperature and wind speed. In order to solve this problem, Zou et al. [24] developed a novel passive air cooling device to provide enough cooling for SCs under the worst case scenario, i.e., high ambient temperature and no wind conditions (Fig. 9.2). The air could be automatically sucked into the channels of aluminum pipes heat sink and took away the waste heat of SCs. Then, the airflow leaving the pipes would be further heated inside the solar collector until it reached the bottom of the chimney, which was used to enhance the chimney effect. Numerical results showed that this novel cooling system could keep cell temperature under 75 °C even as the concentration ratio reached 700 Suns.

9.2.2 Heat Pipe Cooling

Heat pipes are hollow metal pipes consisting of a porous wick material and transport heat by two-phase flow of a working fluid. The liquid working fluid inside the wick is vaporized by the heat in the evaporator section and then flows toward the condenser section carrying the latent heat of vaporization in the tube. The vapor condenses and releases its latent heat in the condenser section, and then returns to the evaporator section through the wick structure by capillary effect. The phase change processes and two-phase flow circulation continue as long as the temperature difference between the evaporator and condenser sections are maintained. Because of the high thermal conductivity and heat transfer characteristics, heat pipe cooling has been used on CPV systems.

Fig. 9.2 Main components of the novel passive air cooling device in Ref. [24]

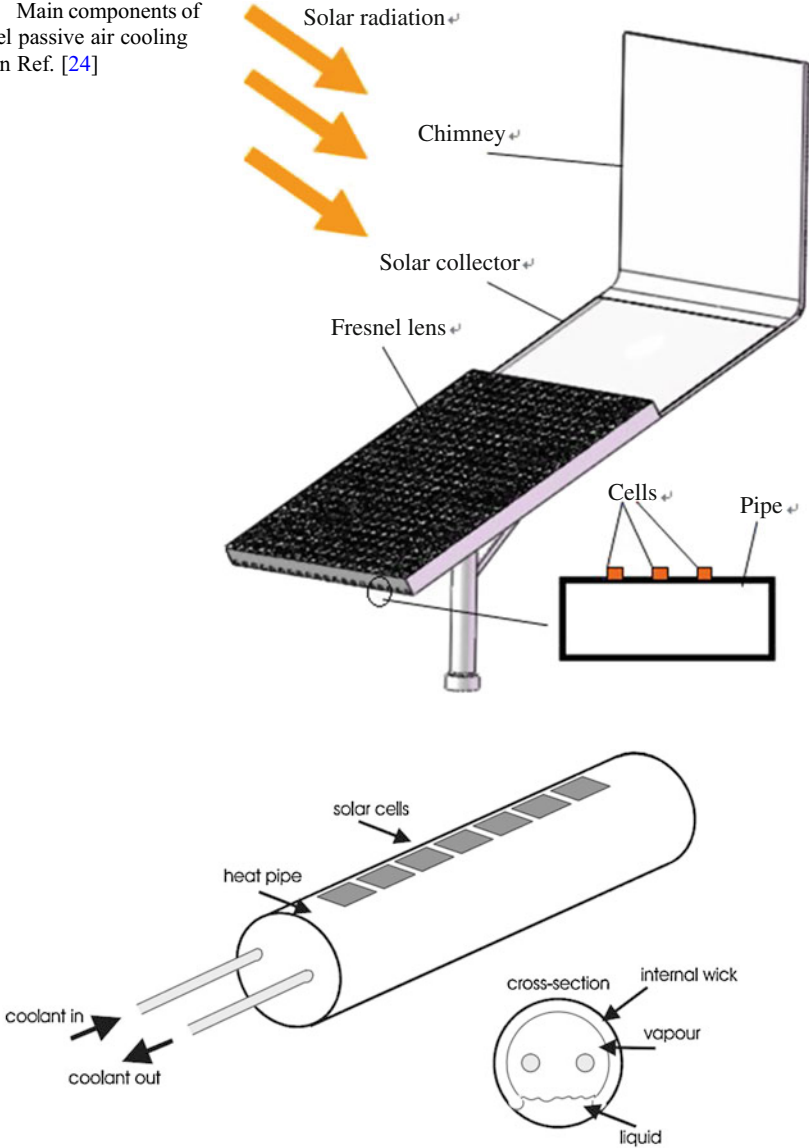


Fig. 9.3 Heat pipe cooling system proposed by Russell [25]

Russell [25] patented a heat pipe cooling system for CPV modules with linear Fresnel lenses. A string of cells mounted along the length of a heat pipe with an internal wick pulling the liquid up to the heated surface (Fig. 9.3). By ensuring a uniform temperature along the pipe, the heat was removed from the heat pipe by an internal coolant circuit. Akbarzadeh and Wadowski [26] experimentally investigated the performance of a heat pipe cooling method for CPV systems at the concentration ratio of

20 Suns. The cell was attached to the evaporator section of the heat pipe, and the upper condenser section extended by fins was exposed to natural convection air cooling. The cooling system was made of copper tube and charged with Freon R-11 [trichloromonofluoromethane, CCl_3F] as the working fluid. The CPV system was exposed to solar radiation for a period of 4 h and it was found that the cell surface temperature did not rise above 46°C . However, the cell surface temperature rose to 84°C and the output power dropped to 10.6 W instead of 20.6 W if the cooling system was not filled with any working fluid. Cheknane et al. [27] also conducted an experimental study regarding the role of heat pipe cooling on silicon-based CPV performance operating up to 500 Suns. The heat pipe cooling system was similar to that used in [26]. Water and acetone were employed as working fluids, and the heat pipe was made of a sealed copper cylinder with fins. The results showed that using acetone in heat pipe cooling improved the performance of SCs at high CR than water. Anderson et al. [28] designed a cooling system that uses a copper heat pipe with aluminum fins to cool a CPV cell by natural convection. They first compared five working fluids (water, ammonia, methanol, toluene, and pentane) for heat pipes and found that water heat pipe with three wraps of 150 mesh screen could carry more than six times heat energy compared to the other working fluids. Then, they determined the optimum fin size that minimized the temperature difference (ΔT , $^\circ\text{C}$) between the CPV cell and ambient air by computational fluid dynamics (CFD) simulation. A copper heater block with cartridge heaters was used to simulate the waste heat from the CPV cell in the experiments. The results showed that the heat pipe rejected the heat with a heat flux of 40 W/cm^2 to the environment with a ΔT rise of only 40°C . Huang et al. [29] proposed and evaluated the performance of a novel hybrid-structure flat plate heat pipe for a CPV (Fig. 9.4). The novel heat pipe was composed of a flattened copper pipe and a sintered wick structure supported by a coronary-stent-like rhombic copper mesh. Experiments presented that the novel heat pipe had less thermal resistance compared to a traditional copper heat pipe. The results also showed that the novel heat pipe provided better performance for a single SC, which could increase the photoelectric conversion efficiency by approximately 3.1%, compared to an aluminum substrate heat sink. Wang et al. [30] numerically and experimentally conducted a comprehensive investigation of the heat pipe cooling for CPV cell thermal management in a concentrator photovoltaics (CPV)/concentrated solar power (CSP) hybrid solar system. The heat transfer performance of three different designs of a

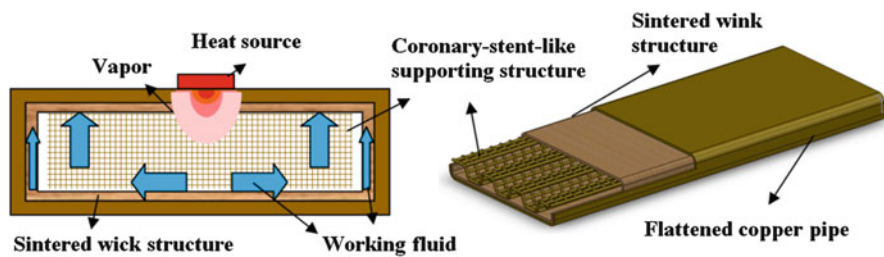


Fig. 9.4 (a) Working mechanism and (b) supporting structure of the novel hybrid-structure flat plate heat pipe in Ref. [29]

single heat pipe with radial fins, double heat pipes with radial fins, and double heat pipes with annular fins was evaluated under various heat rejection requirements. The results showed that heat pipes with radial fins presented narrow capability of dumping the heat, while heat pipes with annular fins had better performances under the same conditions. The double heat pipes with annular fins could bring most of the PV cells to the limited temperature or below under 50 W (13.0 W/cm²) or lower heat load.

9.2.3 Phase Change Material (PCM) Cooling

Phase change material (PCM) which absorb a significant amount of thermal energy as latent heat during the transition from solid to liquid phase are usually incorporated within PV systems for thermal regulation. Appropriately used PCMs can reduce the peak temperature which increases the electrical efficiency by preventing overheating of the system during the daytime. Numerous studies of PV thermal regulation using PCMs have been performed and comprehensively reviewed [31–35]. However, the investigations of CPV systems using PCM are limited.

Sharma et al. [36] presented an experimental investigation of PCM to enhance the thermal performance of very low-concentration building-integrated concentrated photovoltaic (BICPV) systems. The effect of PCM on electrical parameters of the BICPV systems was also discussed. An organic PCM of paraffin wax [(C_nH_{2n} + 2) based (RubiTherm) RT42 (melting temperature 38–43 °C, specific heat capacity 0.2 kJ/kg•K, heat conductivity 0.2 W/m•k] was used to fabricate PCM containment integrated with an in-house manufactured BICPV module. Indoor experiments were conducted with this BICPV-PCM system tested in naturally ventilated mode (without PCM) and then with PCM using highly collimated continuous light source at 1000 W/m². The results showed that stable BICPV temperature of 46.5 °C was achieved with an average temperature reduction of 3.8 °C at the BICPV module center and a relative electrical efficiency improvement of 7.7% with than without PCM. Later, they integrated the micro-fins with PCM and nanomaterial enhanced PCM (n-PCM) for cooling the BICPV systems [37]. In order to overcome PCM leakage, high manufacturing turnaround time, and associated costs, the PCM containment was fabricated using 3-D print technology in this paper. The experimental results showed that the average temperature in the center of the system was reduced by 10.7 °C (15.9%) using micro-fins with PCM and 12.5 °C (18.5%) using micro-fins with n-PCM as compared to using the micro-fins only. However, the n-PCM showed visual signs of agglomeration and deposition of [copper oxide] nano-CuO due to the difference in their densities after successive heating and melting cycles. Emam et al. [38] investigated the performance of an inclined CPV-PCM system using a comprehensive 2-D model comprising of the energy equations for CPV layers and a transient melting-solidification thermo-fluid model for PCM. The effects of inclination angle, concentration ratio, and PCM thickness on the thermal and electrical behaviors of the CPV-PCM system were studied. The results indicated that the system inclination angle had a significant effect on the time required to reach the complete melting state, the transient average solar cell temperature, and temperature

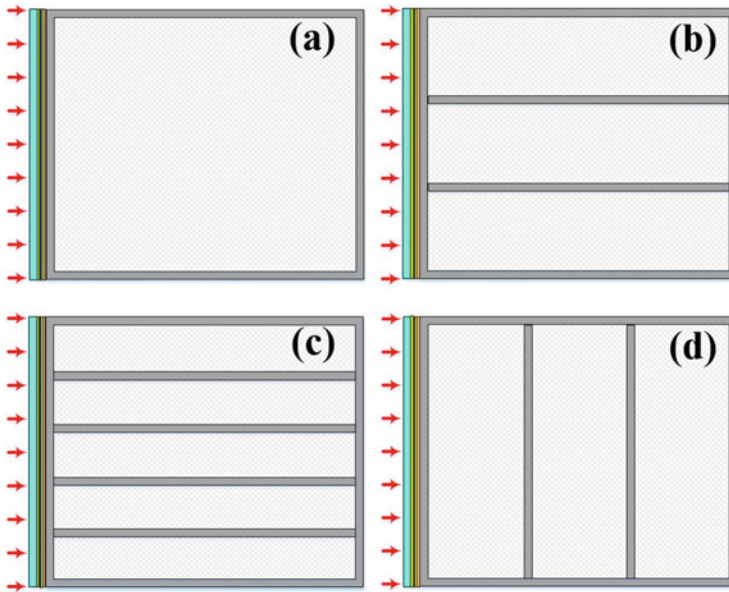


Fig. 9.5 Four different configurations of a PCM heat sink in Ref. [39], (a) a single cavity, (b) three-parallel cavity, (c) five-parallel cavity, and (d) three-series cavity

uniformity. The system at an inclination angle of 45° could reach the minimum average temperature with reasonable uniformity of local solar cell temperature which achieved the highest solar cell electrical efficiency and helped to prevent the hot spots in the solar cell. Later, they developed hybrid CPV-PCM systems to attain rapid thermal dissipation by enhancing the typically low thermal conductivity of PCM [39]. The systems included four different configurations of a PCM heat sink (shown in Fig. 9.5) and nine different pattern arrangements of three PCM materials (n-octadecane paraffin, $\text{CH}_{16}\text{CH}_3$; calcium chloride hexahydrate, $\text{CaCl}_2 \cdot 6\text{H}_2\text{O}$; and eutectic mixture of capric acid/palmitic acid, $\text{C}_{10}\text{H}_{20}\text{O}_2/\text{C}_{16}\text{H}_{32}\text{O}_2$). Using the similar 2-D model, the transient temperature variation at the concentration ratio of 10 and 20 Suns was numerically simulated. The results indicated that the SC temperature decreased with the increasing number of parallel cavities of the PCM heat sink. However, increasing the number of series cavities of PCM heat sink had an unfavorable effect on the SC temperature. Moreover, optimal patterning of PCMs would result in substantial enhancement of the thermal regulation of CPV-PCM systems. Su et al. [40] designed an encapsulated PCM (paraffin wax) spheres immersed in a water tank for a CPV/T system and performed the on-site experiments with a dish concentrator to measure solar irradiance, an output power of SCs and temperatures of the ambient air and water in the collector. The results showed that the average increases of the electrical, thermal, and overall efficiencies for the CPV/T system with PCM cooling were more than 10%, 5%, and 15%, respectively, compared to the CPV/T system with water cooling.

9.3 Active Cooling

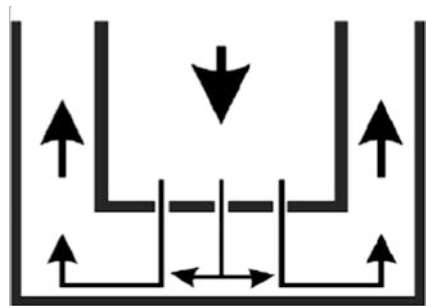
9.3.1 Jet Impingement Cooling

Jet impingement is an attractive cooling technique due to its very low thermal resistances (generally 10^{-5} – 10^{-6} $\text{K}\cdot\text{m}^2/\text{W}$) [41]. The liquid coolant is forced through a narrow hole or slot and impinged onto the heated surface in the normal direction. A very thin thermal boundary layer can be formed in the stagnation zone directly under the impingement and extends radially outward from the jet. As the heat transfer coefficient decreases rapidly with distance from the jet, an array of jets is usually used for cooling large surfaces [8].

Royne and Dey [42] proposed a jet impingement cooling technique for densely packed PV cells under high concentration ratio. Six different jet configurations under arrays of four and nine jets with side drainage normal to the impingement surface (Fig. 9.6) were tested. A model was developed to predict the pumping power required for a given average heat transfer coefficient for different device configurations and found that a higher number of nozzles per unit area improved the performance. They found that cell temperature decreased from 60 °C to 30 °C at the concentration ratio of 200 Suns and from 110 °C to 40 °C for 500 Suns at the maximum power point. Montorfano et al. [43] numerically and experimentally investigated the cells mean temperatures and pressure drop of an impingement water jet cooling system for a CPV cells module. The nozzle to plate distance, the number of jets, the nozzle pitch, and the distance between adjacent jets were optimized through literature and by means of accurate computational fluid dynamics (CFD) simulations. The results showed that the system experienced a pressure drop of 44.03 mbar and the temperature of the cell varied from a minimum of 48.3 °C to a maximum of 51.9 °C at a flow rate of 11 mL/s, a water inlet temperature of 27 °C, and constant incoming power of 150 W.

In order to reduce the temperature nonuniformity inherently induced by the jet impingement distribution, Barrau et al. [44, 45] designed a hybrid jet impingement/microchannel cooling device for densely packed PV cells under high concentration ratio. The device combined a slot jet impingement with a nonuniform distribution of microchannels (Fig. 9.7) and was evaluated by experimental measurements. The results showed that the hybrid device offered a minimum thermal resistance

Fig. 9.6 Schematic drawing of jet configuration with side drainage direction normal to the impingement surface [42]



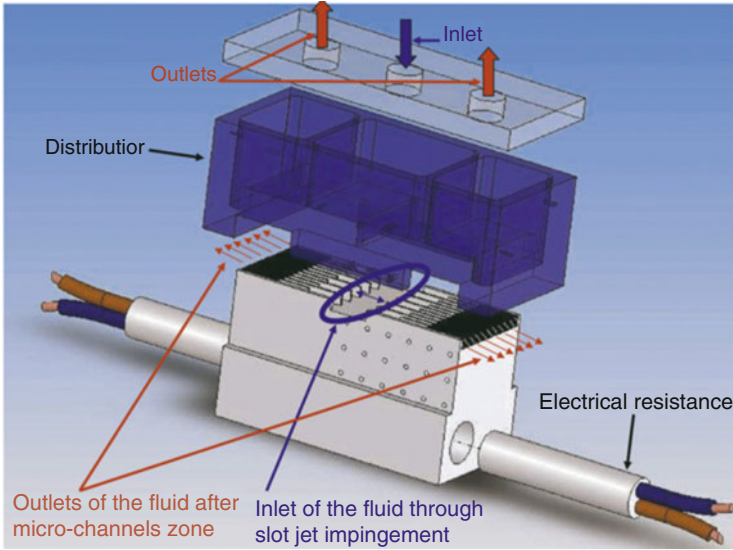


Fig. 9.7 3-D view of the experimental module in Refs. [44, 45]

coefficient of $2.18 \times 10^{-5} \text{ K}\cdot\text{m}^2/\text{W}$ with lower pressure drop and higher net PV output compared to only microchannel cooling. Later, they experimentally tested the efficiency of the hybrid device under real outdoor conditions [46]. A two-stage solar concentrator was used to provide a nonuniform illumination profile on a dummy cell. The results showed that the electrical output of the CPV receiver increased with the water flow rate and concentration ratio. It was indicated that the hybrid device could obtain a high-temperature uniformity of the whole PV receiver by modifying the internal geometry at the design stage to adapt the distribution of the local heat removal capacity.

9.3.2 Liquid Immersion Cooling

With liquid immersion cooling, SCs are directly immersed into the circulating liquid which reduces the contact thermal resistance. The contact thermal resistance is moved to the boundary layer between the bulk liquid and the CPV cell [47]. And the heat can be absorbed by the circulating liquid from both the top and bottom surfaces of the PV cells instead of just the bottom surface.

Zhu et al. [48] proposed a liquid immersion cooling method for densely packed SCs under high concentration ratio. The heat transfer and electrical performances were experimentally investigated under different concentration ratio, liquid temperatures, and flow velocities by using dimethyl-silicon oil as the dielectric fluid. The results showed that the module temperature could be cooled to lower than 45°C and the convective heat transfer coefficient could be higher than $3000 \text{ W}/(\text{m}^2\cdot\text{K})$. A

three-dimensional (3-D) simulation model was established to analyze the detailed velocity and temperature distributions surrounding the cell module. The numerical results indicated that the major heat transfer resistance was due to the laminar layers surrounding the cell and copper substrate. Liu et al. [49] also experimentally investigated the heat dissipation performance of a similar liquid immersion cooling system for SCs module under the conditions of irradiance of 50 and 70 kW/m². The dimethyl-silicon oil was used as the dielectric fluid. The results showed that the liquid inlet temperature had little effect on the module temperature distribution, but had a linear relationship with the average module temperature. The module temperature distribution in turbulent flow was found to be quite uniform, but with some degradation of the electrical performance.

Zhu et al. [50] applied deionized water immersion cooling to a dish high CPV system with a concentration ratio of 250 Suns. Time-dependent temperature distribution and electrical performance of the cell module were experimentally measured. The results showed that the module temperature was reduced to 45 °C at the direct normal irradiance (DNI) of 940 W/m² and 17 °C ambient temperature with 30 °C inlet water temperature. The overall convective heat transfer coefficient was approximately 6000 W/(m²·K). However, the electrical performance of the cell module obviously degraded after a long-time immersion in the deionized water even though its resistivity was kept constant. In order to understand the degradation mechanism, Han et al. [51] conducted the long-term deionized water immersion tests of bare cells, lead based-soldered tabbed cells, and epoxy tabbed cells, respectively. The results showed that the presence of lead oxides (PbO) and tin black oxides (SnO) on the lead based-soldered tabbed cells and red deposition on the epoxy [C₂₁H₂₅ClO₅] tabbed cells confirmed the occurrence of galvanic corrosion, which made the tabbed cells immeasurable finally. However, particular cleaning for the lead based-soldered tabbed cells could recover the (current-voltage) I-V performance toward its initial values, and partial recovery can be obtained for the epoxy tabbed cells, which indicated that the cells were not chemically damaged after long-time deionized water immersion. Xiang et al. [52] used the assembled solar receiver and CPV module prototype in [50] to establish a 3-D numerical simulation model for better understanding the mechanism of the direct-contact heat transfer process. The 3-D simulation model of the liquid-immersed solar receiver and the prototype of a CPV module are shown in Fig. 9.8. The heat transfer performance of the CPV module without and with fins under actual weather conditions was simulated and found that the finned module made the average temperature 8–10 °C lower than the bare one and reduced the temperature nonuniformity from 15 °C to below 10 °C. Sun et al. [53] designed a narrow rectangular channel receiver (Fig. 9.9) to reduce the liquid holdup at the concentration ratio of 9.1 Suns. The experimental results showed that the cell temperature was maintained in the range of 20–31 °C at a direct normal solar irradiance (DNI) of about 910 W/m², silicon oil inlet temperature of 15 °C, and Reynolds number (*Re*) ranging from 2720 to 13,602 (dimensionless). Long-term stability of silicon CPV cells immersed in dimethyl silicon oil was conducted under real climate conditions and found that the cells electrical performance had no obvious efficiency degradation for 270 days of operation.

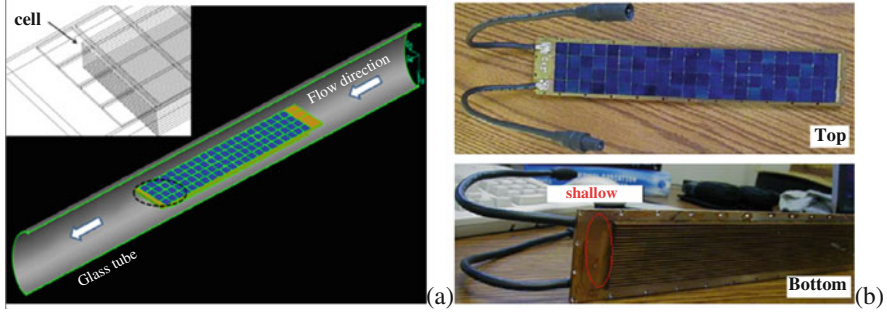


Fig. 9.8 (a) 3-D simulation model of the liquid-immersed solar receiver and (b) prototype of a CPV module in Ref. [52]

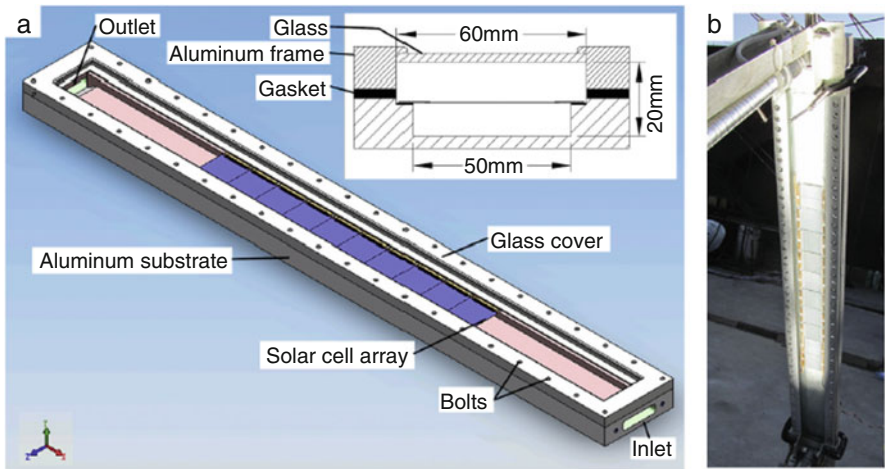


Fig. 9.9 (a) Section view and (b) photo of the narrow rectangular channel receiver in [53]

For purpose of selecting the appropriate dielectric liquid as immersion cooling liquid, Han et al. [47] conducted the optical transmittance measurements of deionized water, isopropyl alcohol, ethyl acetate, and dimethyl silicone oil and found that they all satisfied the optical requirements for silicon CPV applications as immersion coolants. Test cell samples were fabricated by encapsulating between two sheets of 100 mm × 100 mm and 3.3 mm thick Borofloat glass [81% silica, SiO₂; 13% boron oxide, B₂O₃; 4% sodium oxide/potassium oxide, Na₂O/K₂O; and 2% alumina, Al₂O₃], then sealing with silicone to provide a liquid cavity (Fig. 9.10). The electrical performance of silicon CPV cells immersed in those four dielectric liquids was experimental examined using the test cell samples with a constant voltage I-V flash tester. The results showed that the electrical performance of CPV cells improved in the candidate dielectric liquids at the concentration ratio of 10–30 Suns. The light reflection losses and cell surface recombination losses from surface

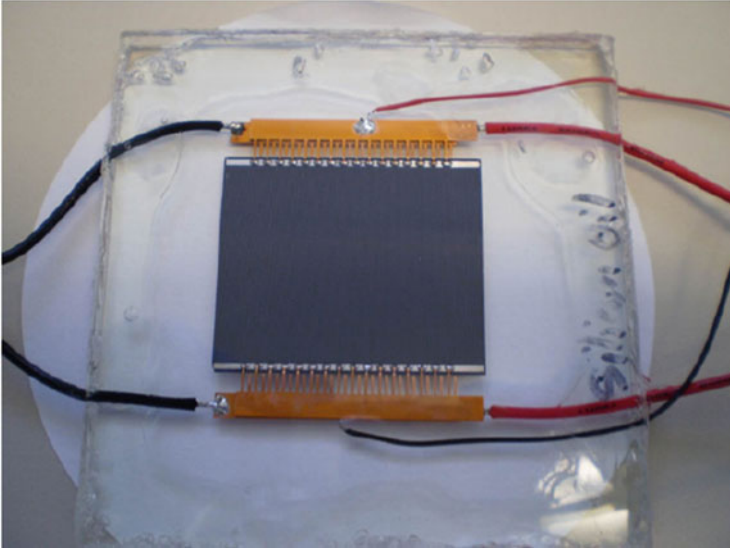


Fig. 9.10 Silicon CPV cell test sample immersed in dimethyl silicon oil used by [47]

adsorption of polar molecules were both reduced. Then, the thermal performance of a liquid immersion cooled solar receiver for a linear CPV system was investigated by numerical simulations and found that the fluid inlet velocity and flow mode, along with the fluid thermal properties, all had significant influences on the cell array temperature. Later, Han et al. [54] investigated the effect of the liquid layer thickness above the cell surface on the electrical performance of silicon CPV cells. The experimental results showed that an increase in the silicon SCs efficiency of 8.5–15.2% was achieved with 1.5 mm liquid thickness immersion, while the degree of the improvements to the efficiency decreased in 9 mm test due to more incident light was absorbed by the thicker liquid layer. And the optimum liquid thickness existed and depended on the liquid types. Long-term cell performance tests demonstrated that the reliable output of the silicon CPV cells was achieved when operated in isopropyl alcohol, ethyl acetate, and dimethyl silicone oil without silicone sealant involved, respectively. However, the stable electrical performance of the cell was difficult to be achieved when immersed in deionized water which was consistent with the report in Ref. [50].

Xin et al. [55] applied the liquid immersion cooling method for GaInP/GaInAs/Ge triple-junction SCs of high CPV systems. They presented that the silicone oil was quite transparent in the wavelength range of both GaInP sub-cell and GaInAs sub-cell, but the transmittances of silicon oil had slightly decreased in the wavelength range of Ge sub-cell. Flash testing showed that the silicon oil immersion could indeed improve the electrical performance of Ge-based MJ cell when the thickness was less than 6.3 mm under 500 Suns and 25 °C. Then, CFD simulation analysis showed that the silicon oil immersion thickness should not be less than 2.5 mm and the cell average temperature

was kept less than 67 °C when the silicon oil mass flow rate was not less than 20 kg/h. Han et al. [56] proposed a theoretical model for the direct liquid-immersed solar receiver with Ge-based MJ CPV cells to investigate the temperature of the receiver and the system electrical efficiency. The results showed that the CR, mass flow rate, and inlet liquid temperature had significant effects on the cell temperature and, by extension, system output power. The flow rate selection should match CR to maintain the cell temperature lower and increase the system electrical efficiency. Kang et al. [57] numerically investigated the heat transfer performance of silicon oil immersion cooling for the densely packed MJ SCs with fins at 500 Suns. The results showed that the cell temperature decreased and the heat transfer coefficient and pressure drop increased with the increasing inlet flow velocity. The cells average temperature was 63 °C, the heat transfer coefficient was 750 W/(m²·K), and the pressure drop was lower than 10 kPa/m when inlet flow velocity and temperature of silicon oil was 1 m/s and 25 °C under the optimized parameters of liquid immersion cooling receiver.

In all immersion cooling systems described above, a high flow rate is usually required to obtain a higher single-phase convective heat transfer due to the high CR and cells temperature, which results in higher parasitic energy consumption. In order to enhance the economic and heat transfer performances, Kang et al. [58] developed a direct-contact phase-change liquid immersion cooling method for dense-array SCs in high CPV system. Ethanol was used as a phase-change immersion cooling liquid. The cooling system could be self-regulating without consuming extra energy with ethanol mass flow rate of 158.3–180.6 kg/(m²·s) under the concentration ratio of 219.8–398.4 Suns. The experimental results showed that the electrical performance of MJ SCs could decline due to the light loss at the interface between ethanol and bubbles. Later, Wang et al. [59] optimized the liquid filling ratio of this cooling system and found that the optimal liquid filling ratio was 30% with the heat transfer coefficient of 9726.21 W/(m²·K).

As the phase-change liquid immersion cooling method generates bubbles which can reduce the cell efficiency and requires higher sealing quality, Wang et al. [60] firstly proposed a direct-contact liquid film cooling system for dense-array SCs in high CPV system. An electric heating plate was designed to simulate the dense-array SCs and water was used as a working fluid. The experimental results showed that the average temperature of simulated SCs and heat transfer coefficient of falling film vaporization both increased with the increasing concentration ratio. Higher water inlet flow rate was found to result in lower average temperature and higher heat transfer coefficient underwater inlet temperature of 30 °C. However, the water inlet flow rate had little impact on average temperature and heat transfer coefficient underwater inlet temperature of 75 °C, which implied that the latent heat transfer became the dominant way of heat transfer. Later, they derived a 2-D model of the direct-contact liquid film cooling system for dense-array SCs to present the temperature distribution on the SCs surface and flow characteristic of the liquid film [61]. The numerical results showed that inlet width had a significant effect on the liquid film thickness. And the subcooled boiling state was a necessary condition to ensure the cooling effect. The optimum inlet parameters at the concentration ratio of 500 Suns were inlet velocity of 1.06 m/s, inlet width of 0.75 mm, and inlet temperature of 75 °C.

9.3.3 Microchannel Heat Sink Cooling

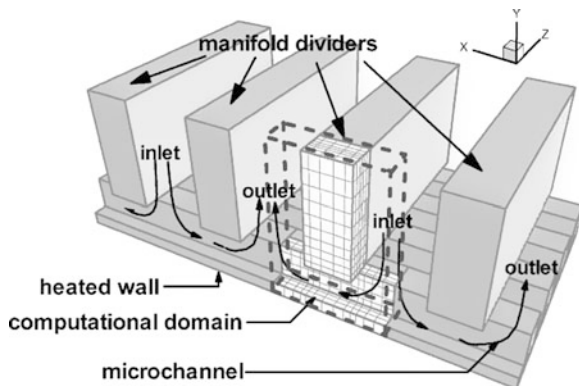
The application of a microchannel heat sink is a potential way to attain extremely high heat transfer rate because of the high surface-area-to-volume ratio of microchannels. Phillips et al. [62] indicated that the use of microchannel cooling system can dissipate heat load as high as 1000 W/cm^2 . Moreover, Royne et al. [8] presented that the microchannel heat sink was a particularly promising cooling technology for high CPV systems. A recent overview of the thermal and hydrodynamic analysis of microchannel heat sinks showed that laminar was the prevailing flow condition and the use of liquid coolants was preferable over gaseous coolants [63].

Ortegón et al. [64] analyzed a microchannel heat sink used for cooling a high CPV cell at the CR of 500 Suns by theoretical and numerical methods. The results indicated that microchannel heat sink cooling was an effective thermal management method for high CPV systems, which improved the cell efficiency to compensate for the higher pressure drop compared to a single rectangular channel heat sink. Capua et al. [65] integrated forward triangular ribs on the inner sidewalls of microchannels to enhance the cooling capability of microchannel heat sinks for a high CPV system. Two structures of aligned and offset distributions along the microchannel walls were considered and investigated in laminar flows by numerical analysis. The results showed that, compared to smooth microchannels, microchannels with aligned and offset rib distributions increased 1.8 and 1.6 times on average Nusselt number (Nu_L , dimensionless), respectively, as well as 3.9 and 2.3 times on average friction factors, respectively. As a relatively high pumping power demand, the microchannel heat sink with forwarding triangular ribs loses its advantage as an effective and efficient cooling system for high CPV application as Re increases, especially at $Re > 200$.

In the conventional microchannel heat sink, liquid coolant temperature can increase along the flow direction resulting in a temperature gradient between the inlet and outlet of the microchannels [66]. To minimize the temperature gradient, a higher coolant flow rate is necessary, which causes higher power consumption. Multi-layer microchannel heat sinks are considered to achieve more efficient cooling in terms of pumping power and heat removal capability [67]. Radwan and Ahmed [68] investigated the influence of microchannel heat sink configurations on the cooling performance of low CPV systems. The numerical results showed that the consumed pumping powers of the double-layer configurations were obviously lower than that of single-layer configurations and achieved a higher net power gain, especially for higher coolant mass flow rates. Siyabi et al. [69] used a 3-D incompressible laminar steady flow model to evaluate the performance of a multi-layer microchannel heat sink for cooling CPV cells. The numerical results showed that an increase in the number of microchannel layers exhibited a significant improvement in terms of SC temperature, the thermal resistance, and the fluid pumping power. Moreover, the channel height and width had no effect on the maximum SC temperature, while increasing channel height resulted in less fluid pumping power.

Another way to decrease the pressure drop and increase the uniformity of temperature distribution of microchannel heat sinks is to use manifold microchannel heat sinks. In a manifold microchannel, the fluid flows in an alternate way through

Fig. 9.11 Schematic of a manifold microchannel heat sink [70]



the direction perpendicular to the heat sink as depicted in Fig. 9.11. As the fluid has a shorter residence time in contact with the base, the uniform temperature distribution across the cooled surface can be obtained [70]. Kermani et al. [71] fabricated and tested a manifold microchannel heat sink for cooling CPV cells under CR of 1000 Suns and used water as the working fluid. The experimental results indicated that the manifold microchannel heat sink could provide high heat transfer coefficient with only moderate pressure drops. Yang and Zuo [72] designed a multi-layer manifold microchannel heat sink to effectively cool the cell surface temperature and improve the uniformity of surface temperature distribution for silicon SC module at CR lower than 100 Suns. The combined use of the multiple inlet/outlet manifolds and plenum chambers increased the fluid flow rate in the inlet area of the microchannels to produce the fluid turbulence which enhanced the heat transfer coefficient. The experimental results showed that the surface temperature difference of the CPV cells was below 6.3 °C. And the multi-layer manifold microchannel had a heat transfer coefficient up to 8235.84 W/(m²•K) and its pressure drop was lower than 3 kPa. Dong et al. [73] proposed a novel mini channel manifold heat sink for densely packed CPVs under CR of 500 Suns by numerical simulations. Two groups of T-shape minichannels were arranged in a manifold heat sink as shown in Fig. 9.12. It was found that the temperature of the maximum cell was lower than 80 °C and the difference between the maximum and minimum temperatures of 100 MJ cells was 26.49 °C when the water inlet velocity was 0.64 m/s.

In addition, two-phase coolants are considered to be used to enhance the cooling performance for microchannel heat sink by increasing the fluid thermal conductivity through using nanofluids or operated under forced convective boiling conditions. Radwan et al. [74] used aluminum oxide (Al₂O₃)-water and silicon carbide (SiC)-water nanofluids with different volume fractions as cooling mediums in a microchannel heat sink for cooling CPV systems. A comprehensive model was developed to estimate the electrical and thermal performances of the CPV systems which included a thermal model for the photovoltaic layers, coupled with thermo-fluid dynamics of two-phase flow model of the microchannel heat sink. The results showed that the use of nanofluids achieved a higher reduction in cell temperature



Fig. 9.12 T-shape manifold with a minichannels heat sink in Ref. [73]

and higher cell electrical efficiency than the use of water, particularly at lower Re and higher concentration ratio. The cell temperature decreased significantly with the increasing volume fraction of nanoparticles. Moreover, using SiC-water nanofluid with higher thermal conductivity had a relatively higher reduction in cell temperature than using Al_2O_3 -water. Later, they experimentally investigated a monolithic double-layer microchannel heat sink used for cooling CPV cells under forced convective boiling conditions [75]. Ethanol [C_2H_5OH] and acetone [C_3H_6O] with a boiling point of $78.4\text{ }^\circ\text{C}$ and $56\text{ }^\circ\text{C}$ were selected as the working fluids. The results showed that there was an excellent uniform temperature around the coolant boiling point over the entire heated wall in a wide range of flow rates. The temperature uniformities were below $1.6\text{ }^\circ\text{C}$ and $1.8\text{ }^\circ\text{C}$ for ethanol and acetone, respectively, under the counterflow operation of forced convective boiling at the CR of 11.5 Suns.

9.4 Discussion and Conclusion Remarks

A comprehensive summary of thermal management techniques for CPV systems has been presented above. As the parameters and performances are quite different for various cooling technologies, the six cooling methods were critically reviewed as listed in Tables 9.1, 9.2, 9.3, 9.4, 9.5, and 9.6.

It can be seen that natural convection heat sink cooling is an effective technique of passive cooling even for high CPV systems. The main drawback of this thermal management technique is that the heat sink area needed to maintain the cell temperature below the nominal operating value increases with the CR which makes the size and weight of CPV modules increase. In tracked CPV system, the weight of heat sink can sensibly affect the overall system performances. The heavier the system, the more the energy consumed by the tracker, and thus, the lower the system's efficiency [20]. Therefore, a large heat sink required to release heat from CPV systems would make the natural convection heat sink less realistic and attractive for cooling. Using fins on the flat plate can significantly improve the cooling capacity so that reduces the volume of a heat sink and also makes the system more compact. Another drawback of this thermal management technique is that ambient conditions such as air temperature and wind speed have major influences on the heat dissipation performance of cooling systems. Even using a very large heat sink, it cannot dissipate enough heat from the CPV module in high ambient temperature and no wind conditions.

Table 9.1 A detailed summary of natural convection heat sink cooling systems

Author (year)	Finned or unfinned	Heat sink dimensions L × W × H (mm ³)	CPV cell dimensions L × W (mm ²)	CPV cell type	The electrical efficiency of CPV cell	CR (Suns)	Cell temperature (°C)	Ambient temperature (°C)	Nature of work
Araki et al. (2002) [13]	Unfinned			Ge-based MJ cell	40%	400 and 500	18 and 21 more than ambient		Experimental
Chou et al. (2007) [14]	Unfinned	535 × 257 × 3	6.7 × 5.5	Ge-based MJ cell	20%	350	44.3	30.5	Numerical
Cui et al. (2009) [16]	Unfinned	700 times larger than SC area	3 × 3	Ge-based MJ cell	22.2%	400	37	27	Analytical
Guladi et al. (2013) [15]	Unfinned	0 × 0 × 3–60 × 60 × 3	2 × 2–10 × 10		40%	> 1000	80		Analytical
Natarajan et al. (2011) [16]	Finned	60 × 20 × 10		Silicon SC	18%	10	49.6	20	Numerical
Micheli et al. (2015) [18]	Finned	110 × 110 × 60	3 × 3	MJ cell	40%	4000	63.3	20	Analytical numerical
Micheli et al. (2015) [19]	Finned	84 × 84 × 56.2	3 × 3	MJ cell	40%	4000	79.3	27.5	Analytical numerical
Micheli et al. (2015) [20]	Finned	50 × 50 × 1.4	3 × 3	Ge-based MJ cell	42.5%	500	70.4	25	Numerical
Aldossary et al. (2016) [11]	Finned	90 × 90 × 52	10 × 10	Ge-based MJ cell	41.2%	500	118 (RPHS) 96 (SFHS)	50	Numerical
Zou et al. (2017) [24]	Unfinned	1400 × 200 × 100			25%	400–700	Under 75	30	Numerical

Table 9.2 A detailed summary of heat pipe cooling systems

Author (year)	Heat pipe structure	CPV cell dimensions $L \times W$ (mm ²)	CPV cell type	The electrical efficiency of CPV cell	CR (Suns)	Cell temperature (°C)	Heat flux for dissipation (W/cm ²)	Ambient temperature (°C)	Nature of work
Russell (1982) [25]	Pipe with the internal coolant circuit								
Akbarzadeh and Wadowski (1996) [26]	Copper pipe with fins	25 × 20	Polycrystalline SCs		20	46			Experimental
Cheknane et al. (2006) [27]	Copper pipe with fins	150	Silicon SC	17–18%	500				Experimental
Anderson et al. (2008) [28]	Copper pipe with aluminum fins	100	Simulated by heater			40 more than ambient	40		Experimental
Huang et al. (2012) [29]	The hybrid-structure flat heat pipe	10 × 10	Ge-based MJ cell	11.2%			40	35	Experimental
Wang et al. (2017) [30]	Copper pipe with fins	14 numbers of 5 × 5.5	Simulated by heater			80	13	35	Numerical experimental

Table 9.3 A detailed summary of CPV-PCM systems

Author (year)	PCM containment dimensions (mm ³)	PCM	CPV cell type	The electrical efficiency of CPV cell	CR (Suns)	Cell temperature (°C)	Ambient temperature (°C)	Nature of work
Sharma et al. (2016) [36]	170 × 160 × 42	RT42	Silicon SC			46.5		Experimental
Sharma et al. (2017) [37]	36 × 35 × 35	RT42 with 0.5% nano-CuO	Simulated by heater				25.6–27.7	Experimental
Emam et al. (2017) [38]	50 or 200 × 125 (2-D)	Calcium chloride hexahydrate CaCl ₂ ·6H ₂ O	Silicon SC	Around 17% for the inclination angles of 45°	5 and 20	Around 80 for the inclination angles of 45°	20	Numerical
Emam and Ahmed (2018) [39]	150 × 125(2-D)	N-octadecane paraffin, calcium chloride hexahydrate CaCl ₂ ·6H ₂ O, eutectic mixture of capric-palmitic acid	Silicon SC	Around 14% for the best	10 and 20	88 for the best	20	Numerical
Su et al. (2018) [40]		Paraffin wax	Silicon SC	Around 40%				Experimental

Table 9.4 A detailed summary of jet impingement cooling systems

Author (year)	CPV cell dimensions L×W (mm ²)	CPV cell type	The electrical efficiency of CPV cell	CR (Suns)	Cell temperature (°C)	Coolant inlet temperature (°C)	Coolant flow rate (L/min)	Thermal resistance (m ² ·K/W)	Nature of work
Roynce and Dey (2007) [42]		Simulated by heater		200 and 500	Around 30 for 200 suns, around 40 for 500 suns			(3.57–3.7) × 10 ⁻⁵ for 200 suns, (2.63–2.7) × 10 ⁻⁵ for 500 suns	Analytical experimental
Montorfano et al. (2014) [43]	5 numbers of 10 × 10	Ge-based MJ cell	37–40%	400–500	48.3–51.9	27	0.22–1.65	1.68 × 10 ⁻⁵	Numerical
Barrau et al. (2010, 2011) [44, 45]	3600	Simulated by heater	30%	1905	Around 40	12.6	32.34	2.18 × 10 ⁻⁵	Experimental
Barrau et al. (2014) [46]	29.75 × 29.75	Dummy cell	39.2%	603 and 861	Around 42 for 603 suns	17.5	1.31–2.94	6.2 × 10 ⁻⁵	Experimental

Table 9.5 A detailed summary of liquid immersion cooling systems

Author (year)	Immersion liquid	CPV cell dimensions $L \times W$ (mm ²)	CPV cell type	The electrical efficiency of CPV cell	CR (Suns)	Cell temperature (°C)	Heat transfer coefficient (W/(m ² ·K))	Coolant inlet temperature (°C)	Coolant flow rate	Nature of work
Zhu et al. (2010) [48]	Dimethyl silicon oil	20 numbers of 5 × 5 in parallel	Silicon SC		160.8 and 202.9	37–57 for 160.8 suns, 40–60 for 202.9 suns	1800–2800 for 160.8 Suns, 2200–3400 for 202.9 Suns	17–28	2–2.8 m/s	Experimental numerical
Han et al. (2011) [47]	Deionized water, isopropyl alcohol, ethyl acetate, and dimethyl silicon oil	10 numbers of 40 × 50 in parallel	Silicon SC		37	31, 52, 41, and 74 for deionized water, isopropyl alcohol, ethyl acetate, and dimethyl silicon oil, respectively		25	4 m ³ /h	Numerical
Liu et al. (2011) [49]	Dimethyl silicon oil	20 numbers of 5 × 5 in parallel	Silicon SC		47.3 and 68.8	30 for 47.3 suns, 45 for 68.6 suns	About 1000 for $Re = 14,194$	17–46	$Re = 1999–14,194$	Experimental
Zhu et al. (2011) [50]	Deionized water	88 numbers of 10 × 10 in series	Silicon SC	24%	250	45	6000	30	2.22 m ³ /h	Experimental
Xiang et al. (2012) [52]	Deionized water	88 numbers of 11 × 11 in series with fins in the back	Silicon SC	24%	250	36.1		24.2	2.23 m ³ /h	Numerical

(continued)

Table 9.5 (continued)

Author (year)	Immersion liquid	CPV cell dimensions $L \times W$ (mm ²)	CPV cell type	The electrical efficiency of CPV cell	CR (Suns)	Cell temperature (°C)	Heat transfer coefficient (W/(m ² ·K))	Coolant inlet temperature (°C)	Coolant flow rate	Nature of work
Sun et al. (2014) [53]	Dimethyl silicone oil	10 numbers of 40×50 in parallel	Silicon SC	19%	9.1	20–31	$Nu = 0.154Re^{0.764}$	15	$Re = 2720-13,602$	Experimental
Xin et al. (2015) [55]	Dimethyl silicone oil	11.01×10.10	Ge-based MJ cell	About 38%	500	About 67		25	20 kg/h	Numerical
Han et al. (2015) [56]	Dimethyl silicone oil	25 numbers of 10×10 in five rows	Ge-based MJ cell	31–33%	100–600	32–97		20	1260–2160 kg/h	Analytical
Kang et al. (2016) [57]	Dimethyl silicone oil	64 numbers of 8×8 in series with fins in the back	Ge-based MJ cell	39.8%	500	63	750	25	1 m/s	Numerical
Kang et al. (2016) [58]	Ethanol	4 numbers of 40×10 in parallel	Simulated by heater	38%	219.8–398.4	87.3–88.5	23,490–46,980		0.245–0.215 m/s	Experimental
Wang et al. (2017) [59]	Deionized water	4 numbers of 40×10 in parallel	Simulated by heater	40%	300–600	65–110	4000–12,000	30–75	$0.1-0.3 \text{ m}^3/\text{h}$	Experimental

Table 9.6 A detailed summary of microchannel heat sink cooling systems

Author (year)	Microchannel heat sink structure	Coolant	CPV cell dimensions $L \times W$ (mm ²)	CPV cell type	The electrical efficiency of CPV cell	CR (Suns)	Cell temperature (°C)	Heat transfer coefficient (W/(m ² ·K))	Coolant inlet temperature (°C)	Coolant flow rate	Nature of work
Kermani et al. (2009) [71]	Multi-layer with manifold	Water		Simulated by heater	25%	1000		65,480		0.3–1.3 gr/s	Experimental
Yang and Zuo (2015) [72]	Multi-layer with manifold	Water	3 numbers of 17×17 in series	Silicon SC		23–98	20–45	1410–8235.84		5.35–37.7 g/s	Experimental
Radwan et al. (2016) [74]	Single layer	Al ₂ O ₃ -water and SiC-water nanofluids			17.5–20%	1–40	Lower than 60		30	$Re = 10–100$	Analytical
Ortegón et al. (2017) [64]	Single layer		10×10		40%	500	45.9		25	$330 \text{ kg}/(\text{m}^2 \cdot \text{K})$	Analytical numerical
Radwan and Ahmed (2017) [68]	Single and multi-layer	Water		Silicon SC	9–15%	5 and 20	80–150		30	$1.67–33.67 \text{ g/s}$	Analytical
Siyabi et al. (2017) [69]	Multi-layer	Water	10×10	Ge-based MJ cell	41.2%	500	Less than 65	Higher than 6000	25	2 g/s	Numerical

(continued)

Table 9.6 (continued)

Author (year)	Microchannel heat sink structure	Coolant	CPV cell dimensions $L \times W$ (mm ²)	CPV cell type	The electrical efficiency of CPV cell	CR (Suns)	Cell temperature (°C)	Heat transfer coefficient (W/(m ² ·K))	Coolant inlet temperature (°C)	Coolant flow rate	Nature of work
Mario Di Capua et al. (2018) [65]	Single layer integrated forward triangular ribs on the inner sidewalls	Water	3 × 3	Ge-based MJ cell	40%	1000	Lower than 28	Higher than 78,125	20	$Re = 100\text{--}400$	Numerical
Radwana et al. (2018) [75]	Multi-layer	Ethanol and acetone	13 × 40	Simulated by heater	20%	11.5	78.4 for ethanol, 56 for acetone			15–400 mL/h	Experimental
Dong et al. (2018) [73]	Single layer with manifold (minichannels)	Water	100 numbers of 10 × 10 in array	Ge-based MJ cell	39.2–40.6%	500	80	7692	34.8	0.64 m/s	Numerical

Heat pipe cooling is another effective passive cooling technique to move and reject heat from CPV modules, especially at low and medium concentration ratio levels. Many investigated works used fins on the heat pipe to improve the cooling capacity. Moreover, as heat pipe operates nearly isothermally, the portion of fins is more effective which needs a smaller volume of fins. Thus, a heat pipe is a good alternative to large natural convection heat sinks, especially when the available space for the cooling system is constrained. However, the use of that technique in terms of economic viability for high CPV systems needs further discussion.

In PCM cooling technology, it is evident from the literature that a limited amount of work has been done for CPV modules in contrast with most of the work done for non-concentrated PVs. The list of various PCMs and their thermal properties that have been used in PV systems is presented in Table 9.7. It can be seen that most PCMs have a low thermal conductivity, which slows their heat charging and discharging rate. The main advantage of using PCM is the ability to regulate temperature based on its latent heat which can result in uniform temperature cooling. Another advantage is its versatility in the choice of melting temperature, and the thickness of the PCM layer can determine the period of time that a relatively stable PV temperature can be maintained. Moreover, using fin designs and optimal patterning of multiple PCM components can also substantially enhance the thermal regulation of CPV-PCM systems. The limitations of using PCM include that some of them are toxic and corrosive, as well as the fire safety and disposal problem after the completion of the life cycle. Further investigations into the applicability of PCM in the thermal management of high CPV module should be conducted, especially in long-term operation.

Jet impingement cooling is an attractive active cooling technique due to its high extraction capability and low thermal resistance. However, as the distance from the jet increases, the heat transfer coefficient decreases rapidly leading to inherent nonuniform temperature distribution. An array of jets is usually used to partially alleviate this problem. But another problem of the disturbance arising from the interaction of the fountain of the jet to another jet can appear and has been shown to decrease the overall heat transfer drastically [76, 77]. The heat transfer characteristics of an array of impinging jets are highly dependent on a plate to nozzle pitch, a number of nozzles, diameter spacing, and fluid velocity which should be well optimized. Moreover, jet impingement with microchannels was shown to enhance the temperature uniformity and can regulate temperature depending upon the local heat removal capacity which makes it an attractive option for cooling CPV modules. Another challenge in the design of such systems is to minimize the pumping power consumption.

In the case of liquid immersion cooling technology, the heat transfer coefficient can go up to $47 \text{ kW}/(\text{m}^2 \cdot \text{K})$. The main applications for such type of cooling reported in the literature are used in densely packed CPV systems with the SCs working under medium and high concentration ratio levels. The common immersion liquid investigated in literature is dimethyl silicone oil, while deionized water was found to have better thermal properties of higher thermal conductivity, heat capacity, and lower viscosity. However, long-term stability tests of silicon CPV cells immersed in those

Table 9.7 List of various PCMs and their thermal properties that have been used in PV systems

PCM	Density (kg/m ³) Solid/ liquid	Specific heat capacity (kJ/(kg·K)) Solid/liquid	Thermal conductivity (W/(m·K)) Solid/liquid	Latent heat of fusion (kJ/kg)	Melting temperature (°C)	Thermal expansion coefficient (1/K)	References
RT18HC	880/770	2	0.2		17–19		[81]
RT20	880/750	1.4/1.7	0.2/0.18	134	21	0.001	[82]
RT25	785/749	1.8/2.4	0.19/0.18	232	26.6	0.001	[83]
RT27	880/760	1.78/2.37	0.2	184	25–28		[84]
RT28HC	880/770	2	0.2	245	28		[85]
RT30	870/760	1.8/2.4	0.2	222	28		[86]
RT35	880/760	1.8/2.4	0.2	157	35		[84]
RT42	800	0.2	0.2	174	38–43		[37]
RT42 with 0.5% nano-CuO	803	0.2	0.36	167–170.5	38.2–43.7		[37]
RT44HC	750	2	0.2	220	44		[87]
RT50	820	2	0.2	130	50		[87]
RT54HC	825	2	0.2	170	54		[87]
SP21E	1500/ 1400	2	0.6		22–23		[81]
SP22	1490/ 1440	1.4/1.95	0.6/0.4	150	23	0.0008	[82]
SP24E	1500/ 1400	2	0.6		24–35		[81]

GR40	710	1.5	0.15	82	43	Almost none	[83]
Waksol A	770/760	2.3/2.43	0.33/0.31	162	32–36		[84]
Calcium chloride hexahydrate $\text{CaCl}_2 \cdot 6\text{H}_2\text{O}$	1710/1560	1.4/2.1	1.08/0.56	191	29.8	0.0005	[38]
N-octadecane paraffin	865/770	1.93/2.16	0.36/0.15	243.5	28	0.00091	[39]
Eutectic mixture of capric-palmitic acid (C-P)	870/790	2/2.3	0.14	173	22.5	0.00078	[39]
Eutectic mixture of capric-lauric acid (C-L)	890/770	1.97/2.24	0.143/0.139	168	18.5	0.00067	[82]
Form-stable paraffin/expanded graphite composite	600		7.57	164.8	27.17		[88]
Pork fat	910/986	2.03/2.05	0.32–0.41	155–180	36–45		[89]

two dielectric fluids present that the electrical performance of the cell had no obvious degradation in dimethyl silicone oil, while obviously degraded in deionized water. But after particular cleaning, the cell could recover. The applications of liquid immersion cooling for Ge-based MJ cells in literature are mainly studied by numerical and analytical methods with none long-term electrical stability test of Ge-based MJ cells immersed in dielectric fluids. Furthermore, the phase-change liquid immersion cooling method was found to have the highest heat transfer coefficient, while the generating bubbles could reduce the cell electrical efficiency. The direct-contact liquid film cooling technology can solve this problem and has a relatively high heat transfer coefficient up to $12 \text{ kW}/(\text{m}^2 \cdot \text{K})$. Stable performance of liquid immersion cooling system for CPV cells under dielectric is a challenging task for future researchers. Moreover, long-term electrical stability tests of Ge-based MJ cells immersed in different dielectric fluids should be conducted to validate whether performance degradation exists or not. And further investigation employing methods such as conformal coating for minimizing the degradation of silicon SCs in deionized water could be conducted.

Microchannel heat sink cooling is also an effective active cooling technique to achieve low cells temperature and uniform temperature distribution of CPV systems. However, it also requires a huge amount of pumping power consumption because of a large pressure drop for the coolant to flow. The use of manifold in microchannel heat sink was reported to enhance cooling capability and minimize the pressure drop due to short microchannels length while allowing the redevelopment of the thermal boundary layer in each channel to obtain high heat transfer coefficients. Moreover, using nanofluid in microchannel heat sink can acquire a significant enhancement in the heat transfer coefficient due to the increase of the mixture of thermal conductivity and the existence of a relative slip/drift velocity between the two phases that eventually enhances the flow mixing [78]. By allowing the coolant fluid in microchannels to boil, a significantly huge heat flux can be dissipated by the latent heat capacity of the fluid and an almost isothermal surface can be obtained. However, the operation temperature of the systems can be slightly higher than the coolant saturation temperature corresponding to the operating pressure [79, 80]. Therefore, the type of coolant should be carefully selected to control the system operating temperature.

Acknowledgments Support from the National Natural Science Foundation of China (51706056) and China Postdoctoral Science Foundation (2018 M631927) is greatly acknowledged.

References

1. L. Micheli, N. Sarmah, X. Luo, K.S. Reddy, T.K. Mallick, Opportunities and challenges in micro-and nano-technologies for concentrating photovoltaic cooling: a review. *Renew. Sust. Energ. Rev.* **20**, 595–610 (2013)
2. S. Jakhar, M.S. Soni, N. Gakkhar, Historical and recent development of concentrating photovoltaic cooling technologies. *Renew. Sust. Energ. Rev.* **60**, 41–59 (2016)

3. K. Lovegrove, W. Stein, *Concentrating Solar Power Technology: Principles, Developments, and Applications* Woodhead Publishing Limited, Cambridge, UK (2012)
4. M. Soni, M. Padmini, Concentrating solar photovoltaic, in *IVth International Conference on Advances in Energy Research* Mumbai, India (2013)
5. I.S.E. Fraunhofer, The new world record for solar cell efficiency at 46% (2014). Press release, Fraunhofer ISE, December 1. Available at <https://www.ise.fraunhofer.de/en/press-media/pressreleases/2014/new-world-record-for-solar-cell-efficiency-at-46-percent.html>. 14 Sept 2017
6. M.A. Green, K. Emery, Y. Hishikawa, W. Warta, E.D. Dunlop, D.H. Levi, et al., Solar cell efficiency tables (version 49). *Prog. Photovolt. Res. Appl.* **25**, 565–572 (2010)
7. P. Pérez-Higueras, E. Muñoz, G. Almonacid, P.G. Vidal, High concentrator photovoltaics efficiencies: Present status and forecast. *Renew. Sustain. Energy Rev.* **15**(4), 1810–1815 (2011)
8. A. Royne, C.J. Dey, D.R. Mills, Cooling of photovoltaic cells under concentrated illumination: a critical review. *Sol. Energy Mater. Sol. Cells* **86**(4), 451–483 (2005)
9. Z. Ye, Q. Li, Q. Zhu, W. Pan, The cooling technology of solar cells under a concentrated system, in *Proceedings of the IEEE 6th International Power Electro and Motion Control Conference, IPEMC'09*, 3 Wuhan, China (2009), pp. 2193–2197
10. E. Skoplaki, J.A. Palyvos, On the temperature dependence of photovoltaic module electrical performance: a review of efficiency/power correlations. *Sol. Energy* **83**(5), 614–624 (2009)
11. A. Aldossary, S. Mahmoud, R. Al-Dadah, Technical feasibility study of passive and active cooling for concentrator PV in a harsh environment. *Appl. Therm. Eng.* **100**, 490–500 (2016)
12. K. Nashik, T. Takamoto, T. Agui, M. Kaneiwa, Y. Uraoka, T. Fuyuki, Annual output estimation of concentrator photovoltaic systems using high-efficiency gap/in GaAs/Ge triple-junction solar cells based on experimental solar cell's characteristics and field-test meteorological data. *Sol. Energy Mater. Sol. Cells* **90**(1), 57–67 (2006)
13. K. Araki, H. Uozumi, M. Yamaguchi, A simple passive cooling structure and its heat analysis for 500× concentrator PV module, in *Photovoltaic Specialists Conference, 2002. Conference Record of the Twenty-Ninth IEEE*, New Orleans, Los Angeles, USA, vol. 18 (IEEE, 2002), pp.1568–1571
14. T. L. Chou, Z. H. Shih, H. F. Hong, C. N. Han, Investigation of the thermal performance of high-concentration photovoltaic solar cell package, in *International Conference on Electronic Materials and Packaging Daejeon*, South Korea (IEEE, 2007), pp. 1–6
15. F. Gualdi, O. Arenas, A. Vossier, A. Dollet, V. Aimez, R. Arès, Determining passive cooling limits in CPV using an analytical thermal model, *9th International Conference on Concentrator Photovoltaic Systems*, Miyazaki, Japan, AIP Conference Proceeding. **1556**(48), 10–13 (2013)
16. M. Cui, N.F. Chen, X.L. Yang, Y. Wang, Y.N. Bai, X.W. Zhang, Thermal analysis and test for single concentrator solar cells. *J. Semicond.* **30**(4), 63–66 (2009)
17. S.K. Natarajan, T.K. Mallick, M. Katz, S. Weingaertner, Numerical investigations of solar cell temperature for photovoltaic concentrator system with and without passive cooling arrangements. *Int. J. Therm. Sci.* **50**(12), 2514–2521 (2011)
18. L. Micheli, E.F. Fernandez, F. Almonacid, K.S. Reddy, T.K. Mallick, *Enhancing Ultra-High CPV Passive Cooling Using Least-Material Finned Heat Sinks*, American Institute of Physics Conference Series, vol 1679 (AIP Publishing LLC, 2015), pp. 1810–001575
19. L. Micheli, E. F. Fernández, F. Almonacid, K. S. Reddy, T. K. Mallick, Optimization of the least-material approach for passive Ultra-High CPV cooling, in *Photovoltaic Specialist Conference*, New Orleans, Los Angeles, USA (IEEE, 2015), pp. 1–6
20. L. Micheli, S. Senthilarasu, K.S. Reddy, T.K. Mallick, Applicability of silicon micro-finned heat sinks for 500× concentrating photovoltaic systems. *J. Mater. Sci.* **50**(16), 5378–5388 (2015)
21. K.H. Do, T.H. Kim, Y.S. Han, B.I. Choi, M.B. Kim, A general correlation of a natural convective heat sink with plate-fins for high concentrating photovoltaic module cooling. *Sol. Energy* **86**(9), 2725–2734 (2012)
22. A. Bar-Cohen, M. Iyengar, A.D. Kraus, Design of optimum plate-fin natural convective heat sinks. *J. Electron. Packag.* **125**(2), 208–216 (2003)

23. A. Dayan, R. Kushnir, G. Mittelman, A. Ullmann, Laminar free convection underneath a downward facing hot fin array. *Int. J. Heat Mass Transfer* **47**(12), 2849–2860 (2004)
24. Z. Zou, H. Gong, J. Wang, S. Xie, Numerical investigation of solar enhanced passive air cooling system for concentration photovoltaic module heat dissipation. *J. Clean Energy Technol.* **5**(3) 206–211 (2017)
25. G. F. Russell, U.S. Patent No. 4,320,246, 1982. U.S. Patent and Trademark Office, Washington, DC
26. A. Akbarzadeh, T. Wadowski, Heat pipe-based cooling systems for photovoltaic cells under concentrated solar radiation. *Appl. Therm. Eng.* **16**(1), 81–87 (1996)
27. A. Chekane, B. Benyoucef, A. Chaker, Performance of concentrator solar cells with passive cooling. *Semicond. Sci. Technol.* **21**(2), 144 (2006)
28. W. G. Anderson, P. M. Dussinger, D. B. Sarraf, S. Tamanna, Heat pipe cooling of concentrating photovoltaic cells, in *Photovoltaic Specialists Conference*, 2008. PVSC'08. 33rd IEEE (IEEE, 2008, May), San Diego, California, USA, pp. 1–6
29. H.J. Huang, S.C. Shen, H.J. Shaw, Design and fabrication of a novel hybrid-structure heat pipe for a concentrator photovoltaic. *Energies* **5**(11), 4340–4349 (2012)
30. S. Wang, J. Shi, H. H. Chen, S. R. Schafer, M. Munir, G. Stecker, . . . , C. L. Chen, Cooling design and evaluation for photovoltaic cells within constrained space in a CPV/CSP hybrid solar system. *Appl. Therm. Eng.* **110**, 369–381 (2017)
31. M.C. Browne, B. Norton, S.J. McCormack, Phase change materials for photovoltaic thermal management. *Renew. Sust. Energ. Rev.* **47**, 762–782 (2015)
32. T. Ma, H. Yang, Y. Zhang, L. Lu, X. Wang, Using phase change materials in photovoltaic systems for thermal regulation and electrical efficiency improvement: a review and outlook. *Renew. Sust. Energ. Rev.* **43**, 1273–1284 (2015)
33. M.M. Islam, A.K. Pandey, M. Hasanuzzaman, N.A. Rahim, Recent signs of progress and achievements in photovoltaic-phase change material technology: a review with special treatment on photovoltaic thermal-phase change material systems. *Energy Convers. Manag.* **126**, 177–204 (2016)
34. S.S. Chandel, T. Agarwal, Review of cooling techniques using phase change materials for enhancing the efficiency of photovoltaic power systems. *Renew. Sust. Energ. Rev.* **73**, 1342–1351 (2017)
35. S. Preet, Water and phase change material based photovoltaic thermal management systems: a review. *Renew. Sust. Energ. Rev.* **82**, 791–807 (2018)
36. S. Sharma, A. Tahir, K.S. Reddy, T.K. Mallick, Performance enhancement of a building-integrated concentrating photovoltaic system using phase change material. *Sol. Energy Mater. Sol. Cells* **149**, 29–39 (2016)
37. S. Sharma, L. Micheli, W. Chang, A.A. Tahir, K.S. Reddy, T.K. Mallick, Nano-enhanced phase change material for thermal management of BICPV. *Appl. Energy* **208**, 719–733 (2017)
38. M. Emam, S. Ookawara, M. Ahmed, Performance study and analysis of an inclined concentrated photovoltaic-phase change material system. *Sol. Energy* **150**, 229–245 (2017)
39. M. Emam, M. Ahmed, Cooling concentrator photovoltaic systems using various configurations of phase-change material heat sinks. *Energy Convers. Manag.* **158**, 298–314 (2018)
40. Y. Su, Y. Zhang, L. Shu, Experimental study of using phase change material cooling in a solar tracking concentrated photovoltaic-thermal system. *Sol. Energy* **159**, 777–785 (2018)
41. W. M. Rohsenow, Y. I. Cho, in *Handbook of Heat Transfer*, ed. by J. P. Hartnett, vol. 3 (McGraw-Hill, New York, 1998)
42. A. Roynce, C.J. Dey, Design of a jet impingement cooling device for densely packed PV cells under high concentration. *Sol. Energy* **81**(8), 1014–1024 (2007)
43. D. Montorfano, A. Gaetano, M. C. Barbato, G. Ambrosetti, A. Pedretti, CPV cells cooling system based on submerged jet impingement: CFD modeling and experimental validation, in *AIP Conference Proceedings*, vol. 1616, No. 1 (AIP, 2014), Albuquerque, New Mexico, USA, pp. 135–139

44. J. Barrau, J. Rosell, M. Ibañez, Design of a hybrid jet impingement/microchannel cooling device for densely packed PV cells under high concentration, in *AIP Conference Proceedings*, vol. 1277, No. 1 (AIP, 2010), Freiburg, Germany, pp. 74–77
45. J. Barrau, J. Rosell, D. Chemisana, L. Tadriss, M. Ibañez, Effect of a hybrid jet impingement/micro-channel cooling device on the performance of densely packed PV cells under high concentration. *Sol. Energy* **85**(11), 2655–2665 (2011)
46. J. Barrau, A. Perona, A. Dollet, J. Rosell, Outdoor test of a hybrid jet impingement/micro-channel cooling device for densely packed concentrated photovoltaic cells. *Sol. Energy* **107**, 113–121 (2014)
47. X. Han, Y. Wang, L. Zhu, Electrical and thermal performance of silicon concentrator solar cells immersed in dielectric liquids. *Appl. Energy* **88**(12), 4481–4489 (2011)
48. L. Zhu, Y. Wang, Z. Fang, Y. Sun, Q. Huang, An effective heat dissipation method for densely packed solar cells under high concentrations. *Sol. Energy Mater. Sol. Cells* **94**(2), 133–140 (2010)
49. L. Liu, L. Zhu, Y. Wang, Q. Huang, Y. Sun, Z. Yin, Heat dissipation performance of silicon solar cells by direct dielectric liquid immersion under intensified illuminations. *Sol. Energy* **85**(5), 922–930 (2011)
50. L. Zhu, R.F. Boehm, Y. Wang, C. Halford, Y. Sun, Water immersion cooling of PV cells in a high concentration system. *Sol. Energy Mater. Sol. Cells* **95**(2), 538–545 (2011)
51. X. Han, Y. Wang, L. Zhu, H. Xiang, H. Zhang, Mechanism study of the electrical performance change of silicon concentrator solar cells immersed in de-ionized water. *Energy Convers. Manag.* **53**(1), 1–10 (2012)
52. H. Xiang, Y. Wang, L. Zhu, X. Han, Y. Sun, Z. Zhao, 3D numerical simulation on heat transfer performance of a cylindrical liquid immersion solar receiver. *Energy Convers. Manag.* **64**, 97–105 (2012)
53. Y. Sun, Y. Wang, L. Zhu, B. Yin, H. Xiang, Q. Huang, Direct liquid-immersion cooling of concentrator silicon solar cells in a linear concentrating photovoltaic receiver. *Energy* **65**, 264–271 (2014)
54. X. Han, Y. Wang, L. Zhu, The performance and long-term stability of silicon concentrator solar cells immersed in dielectric liquids. *Energy Convers. Manag.* **66**, 189–198 (2013)
55. G. Xin, Y. Wang, Y. Sun, Q. Huang, L. Zhu, Experimental study of liquid-immersion III–V multi-junction solar cells with dimethyl silicone oil under high concentrations. *Energy Convers. Manag.* **94**, 169–177 (2015)
56. X. Han, Q. Wang, J. Zheng, J. Qu, Thermal analysis of direct liquid-immersed solar receiver for a high concentrating photovoltaic system. *Int. J. Photoenergy* (2015)
57. X. Kang, Y.P. Wang, G.C. Xin, X.S. Shi, Experiment and simulation study on silicon oil immersion cooling densely-packed solar cells under high concentration ratio. *Int. J. Energy Power Eng.* **5**(3), 90–96 (2016)
58. X. Kang, Y. Wang, Q. Huang, Y. Cui, X. Shi, Y. Sun, Study on direct-contact phase-change liquid immersion cooling dense-array solar cells under high concentration ratios. *Energy Convers. Manage.* **128**, 95–103 (2016)
59. Y. Wang, C. Wen, Q. Huang, X. Kang, M. Chen, H. Wang, Performance comparison between ethanol phase-change immersion and active water cooling for solar cells in a high concentrating photovoltaic system. *Energy Convers. Manage.* **149**, 505–513 (2017)
60. Y. Wang, X. Shi, Q. Huang, Y. Cui, X. Kang, Experimental study on direct-contact liquid film cooling simulated dense-array solar cells in the high concentrating photovoltaic system. *Energy Convers. Manage.* **135**, 55–62 (2017)
61. Y. Wang, L. Zhou, X. Kang, Q. Huang, X. Shi, C. Wang, Experimental and numerical optimization of direct-contact liquid film cooling in high concentration photovoltaic system. *Energy Convers. Manage.* **154**, 603–614 (2017)
62. L. R. Glicksman, R. L. R. J. Phillips, Forced-convection, liquid cooled; microchannel heat sinks for high power-density microelectronics, in *Proceedings of the International Symposium on Cooling Technology for Electronic Equipment* (1987), pp. 295–316

63. A.M. Adham, N. Mohd-Ghazali, R. Ahmad, Thermal and hydrodynamic analysis of micro-channel heat sinks a review. *Renew. Sustain. Energy Rev.* **21**(21), 614–622 (2013)
64. J. A. A. Ortegón, J. P. Cassiano, E. M. Cardoso, J. B. C. Silva, CFD analysis of a microchannel heat sink cooling system for high concentration photovoltaic systems, in *Cilamce*, Florianópolis, SC, Brazil, November, 5–8 (2017)
65. M.D.H. Capua, R. Escobar, A.J. Diaz, A.M. Guzmán, Enhancement of the cooling capability of a high concentration photovoltaic system using microchannels with forwarding triangular ribs on sidewalls. *Appl. Energy* **226**, 160–180 (2018)
66. K. Vafai, L. Zhu, Analysis of two-layered micro-channel heat sink concept in electronic cooling. *Int. J. Heat Mass Transf.* **42**(12), 2287–2297 (1999)
67. X. Wei, Y. Joshi, Stacked microchannel heat sinks for liquid cooling of microelectronic components. *J. Electron. Packag.* **126**(1), 60–66 (2004)
68. A. Radwan, M. Ahmed, The influence of microchannel heat sink configurations on the performance of low concentrator photovoltaic systems. *Appl. Energy* **206**, 594–611 (2017)
69. I. A. Siyabi, K. Shanks, T. Mallick, S. Sundaram, Thermal analysis of a multi-layer micro-channel heat sink for cooling concentrator photovoltaic (CPV) cells, in *AIP Conference Proceedings*, vol. 1881, No. 1 (AIP Publishing, 2017), Ottawa, Canada, p. 070001
70. J.H. Ryu, D.H. Choi, S.J. Kim, Three-dimensional numerical optimization of a manifold microchannel heat sink. *Int. J. Heat Mass Transf.* **46**(9), 1553–1562 (2003)
71. E. Kermani, S. Dessiatoun, A. Shooshtari, M. M. Ohadi, Experimental investigation of heat transfer performance of a manifold microchannel heat sink for cooling of concentrated solar cells, in *Electronic Components and Technology Conference, 2009. ECTC 2009. 59th* (IEEE, 2009), San Diego, California, USA pp. 453–459
72. K. Yang, C. Zuo, A novel multi-layer manifold microchannel cooling system for concentrating photovoltaic cells. *Energy Convers. Manag.* **89**, 214–221 (2015)
73. J. Dong, X. Zhuang, X. Xu, Z. Miao, B. Xu, Numerical analysis of a multi-channel active cooling system for densely packed concentrating photovoltaic cells. *Energy Convers. Manag.* **161**, 172–181 (2018)
74. A. Radwan, M. Ahmed, S. Ookawara, Performance enhancement of concentrated photovoltaic systems using a microchannel heat sink with nanofluids. *Energy Convers. Manag.* **119**, 289–303 (2016)
75. A. Radwan, S. Ookawara, S. Mori, M. Ahmed, Uniform cooling for concentrator photovoltaic cells and electronic chips by forced convective boiling in a 3D-printed monolithic double-layer microchannel heat sink. *Energy Convers. Manag.* **166**, 356–371 (2018)
76. B. W. Webb, C. F. Ma, Single-phase liquid jet impingement heat transfer, in *Advances in Heat Transfer*, vol. 26 (Elsevier, 1995), Salt Lake City, Utah, USA, pp. 105–217
77. D.Y. Lee, K. Vafai, Comparative analysis of jet impingement and microchannel cooling for high heat flux applications. *Int. J. Heat Mass Transf.* **42**(9), 1555–1568 (1999)
78. M. Ahmed, M. Eslamian, Laminar forced convection of a nanofluid in a microchannel: effect of flow inertia and external forces on heat transfer and fluid flow characteristics. *Appl. Therm. Eng.* **78**, 326–338 (2015)
79. C. Huh, M.H. Kim, An experimental investigation of flow boiling in an asymmetrically heated rectangular microchannel. *Exp. Thermal Fluid Sci.* **30**(8), 775–784 (2006)
80. L. Yin, R. Xu, P. Jiang, H. Cai, L. Jia, Subcooled flow boiling of water in a large aspect ratio microchannel. *Int. J. Heat Mass Transf.* **112**, 1081–1089 (2017)
81. W. Lin, Z. Ma, P. Cooper, M.I. Sohel, L. Yang, Thermal performance investigation and optimization of buildings with integrated phase change materials and solar photovoltaic thermal collectors. *Energ. Buildings* **116**, 562–573 (2016)
82. A. Hasan, S.J. McCormack, M.J. Huang, B. Norton, Characterization of phase change materials for thermal control of photovoltaics using differential scanning calorimetry and temperature history method. *Energy Convers. Manag.* **81**, 322–329 (2014)
83. M.J. Huang, P.C. Eames, B. Norton, Phase change materials for limiting temperature rise in building integrated photovoltaics. *Sol. Energy* **80**(9), 1121–1130 (2006)

84. M.J. Huang, P.C. Eames, B. Norton, N.J. Hewitt, Natural convection in an internally finned phase change material heat sink for the thermal management of photovoltaics. *Sol. Energy Mater. Sol. Cells* **95**(7), 1598–1603 (2011)
85. U. Stritih, Increasing the efficiency of PV panel with the use of PCM. *Renew. Energy* **97**, 671–679 (2016)
86. S. Preet, B. Bhushan, T. Mahajan, Experimental investigation of water-based photovoltaic/thermal (PV/T) system with and without phase change material (PCM). *Sol. Energy* **155**, 1104–1120 (2017)
87. T. Klemm, A. Hassabou, A. Abdallah, O. Andersen, Thermal energy storage with phase change materials to increase the efficiency of solar photovoltaic modules. *Energy Procedia* **135**, 193–202 (2017)
88. Z. Luo, Z. Huang, N. Xie, X. Gao, T. Xu, Y. Fang, Z. Zhang, Numerical and experimental study on temperature control of solar panels with form-stable paraffin/expanded graphite composite PCM. *Energy Convers. Manag.* **149**, 416–423 (2017)
89. S. Nižetić, M. Arıcı, F. Bilgin, F. Grubišić-Čabo, Investigation of pork fat as potential novel phase change material for passive cooling applications in photovoltaics. *J. Clean. Prod.* **170**, 1006–1016 (2018)